

Domain Dependent Fermi Arcs Observed in a Striped Phase Dichalcogenide

Takashi Mizokawa,* Alexei Barinov, Viktor Kandyba, Alessio Giampietri, Ryoya Matsumoto, Yohei Okamoto, Kou Takubo, Koji Miyamoto, Taichi Okuda, Sunseng Pyon, Hiroyuki Ishii, Kazutaka Kudo, Minoru Nohara, and Naurang L. Saini*

Solids undergoing symmetry breaking phase transitions commonly exhibit domains of low symmetry phases with various sizes and morphological shapes. Usually, the shapes of these domains are not directly related to the nature of symmetry breaking. Here, an interesting example of a layered dichalcogenide with a triangular lattice is shown, in which symmetry breaking of electronic charge/orbital is accompanied by formation of striped domains and exotic surface states with peculiar spin textures. Using angle-resolved photoemission spectromicroscopy, the mesoscopic striped domains in the layered IrTe_2 are observed across the first order phase transition at ≈ 280 K. Under further cooling down to 47 K, the striped domains evolve into trijunction domains with electronic anisotropy in three directions. Each domain harbors quasi 1D surface bands forming fragmented Fermi surfaces (Fermi arcs) with peculiar spin polarization revealed by spin-resolved photoemission spectroscopy. The Fermi arc corresponds to an edge state of the 2D bulk electronic bands truncated at the surface, indicating an interesting interplay between the symmetry breaking, surface electronic structure, and the spin state.


1. Introduction

Domain structures in bistable or polystable electronic systems exhibit various morphological shapes that have been one of the subjects of frontier research in fundamental science of advanced materials. Some fascinating examples include the topological domain textures in multiferroic YMnO_3 ^[1,2] and antiferromagnetic Fe_2O_3 ^[3] revealed by electron microscopy and photoemission electron microscopy. Other interesting examples are the antiferromagnetic $\text{Nd}_2\text{Ir}_2\text{O}_7$ ^[4] and multiferroic BiFeO_3 ^[5,6] showing domain wall properties discovered, respectively, by scanning microwave impedance microscopy and conductive atomic force microscopy. In systems showing Mott transitions and colossal magnetoresistance, metallic and insulating domains have also been disclosed by photoemission spectromicroscopy.^[7,8] In general,

mesoscopic domain structures of symmetry-broken electronic systems are not directly related to the nature of the broken symmetry itself but determined by the interfacial energy minimum.

T. Mizokawa, R. Matsumoto, Y. Okamoto
Department of Applied Physics
Waseda University
Shinjuku, Tokyo 169-8555, Japan
E-mail: mizokawa@waseda.jp
A. Barinov, V. Kandyba, A. Giampietri
Sincrotrone Trieste S.C.p.A.
Area Science Park, Basovizza, Trieste 34012, Italy
K. Takubo
Department of Chemistry
Tokyo Institute of Technology
Meguro, Tokyo 152-8551, Japan
K. Miyamoto, T. Okuda
Hiroshima Synchrotron Radiation Center
Hiroshima University
Hiroshima 739-0046, Japan

S. Pyon
Department of Applied Physics
The University of Tokyo
Bunkyo, Tokyo 113-8656, Japan
H. Ishii
Department of Physics
Okayama University
Okayama 700-8530, Japan
K. Kudo
Department of Physics
Osaka University
Toyonaka, Osaka 560-0043, Japan
M. Nohara
Department of Quantum Matter
Hiroshima University
Hiroshima 739-8530, Japan
N. L. Saini
Department of Physics
Università di Roma "La Sapienza,"
Rome 00185, Italy
E-mail: naurang.saini@roma1.infn.it

 The ORCID identification number(s) for the author(s) of this article can be found under <https://doi.org/10.1002/qute.202200029>

DOI: 10.1002/qute.202200029

Therefore, morphology of the domains in these systems are not associated with the underlying lattice direction. A rare case is the shape memory alloys, namely NiMn_2Ga , in which the symmetry-broken electronic state is associated with the domain texture and the shape memory effect.^[9] However, it is difficult to study their domain dependent electronic states due to the 3D nature. In this context, it is highly interesting to explore if the morphology of domains has any direct relationship with the symmetry breaking in quasi 2D materials which can provide flat surfaces. Another important aspect of the quasi 2D materials is emergence of spin-polarized surface states. If spin-polarized surface states are associated with the domain formation, such materials would be a fascinating platform for spin manipulation by temperature, local strain, and more.

Among various systems showing first-order phase transitions, CuIr_2S_4 with an Ir pyrochlore lattice manifests a transition with octamer charge order,^[10] which is accompanied by a dramatic Ir 5d orbital symmetry breaking.^[11] The layered IrTe_2 with a triangular lattice of Ir exhibits a structural phase transition from trigonal to monoclinic or triclinic,^[12,13] similar to that of CuIr_2S_4 , at ≈ 280 K. As the layered IrTe_2 crystals can be cleaved to obtain flat surfaces, IrTe_2 is best suited for photoemission studies unlike CuIr_2S_4 . The single crystal samples of IrTe_2 reveal two structural phase transitions around 280 and 180 K.^[14] In addition, there seems an interesting interplay between the structural phase transition and superconductivity in IrTe_2 ^[15,16] in which multi-band Fermi surfaces are expected to play a significant role.^[17] An optical study has shown that the band structure is reconstructed over a broad energy scale up to ≈ 2 eV indicating importance of the Te 5p orbitals together with the Ir 5d orbitals.^[18–20] The interplay between the Ir 5d and Te 5p orbitals is essential that has also been indicated by extended X-ray absorption fine structure, photoemission, and high pressure studies.^[21–24] The stripe-type charge/orbital order in IrTe_2 was identified by X-ray diffraction and ab initio calculations,^[25–27] and further indicated in scanning tunneling microscopy studies^[28–31] as well as in a soft-X-ray scattering study.^[32] In particular, the study by Mauere et al. revealed domain boundaries at which the charge/orbital stripes are truncated.^[30] More recently, complex phase evolution due to a heterogeneous nucleation mechanism has been revealed by scanning Raman microscopy.^[33] In the charge/orbital ordered phase, it is expected that each domain is characterized by an anisotropic electronic state driven by the anisotropic charge/orbital order with Ir^{4+} -like dimerized sites forming stripes as illustrated in **Figure 1a**. The Ir–Ir dimers are arranged to form the stripes running along one of the trigonal axes.

The bulk electronic states under the stripe-type charge/orbital order provide quasi 2D Fermi surfaces.^[25–27] The direction of the quasi 2D is tilted from the c-axis of the trigonal phase as shown in **Figure S1a**, Supporting Information. The Fermi surfaces of the charge/orbital ordered phase have been studied by angle-resolved photoemission spectroscopy.^[20,34–37] The comparison between the theory and the experiment is shown in **Figure S1a,b**, Supporting Information. In particular, the electron pockets around the bulk X point were theoretically predicted^[25–27] and experimentally confirmed.^[34] The quasi 1D Fermi surfaces, which were first reported by Ootsuki et al.,^[20] have been confirmed to have surface origin from their photon energy dependence.^[35] The quasi 1D surface bands are apparently disconnected from the bulk electron

bands.^[35–37] As a result, the Fermi surfaces created by the surface bands are fragmented and somewhat similar to the Fermi arcs observed in underdoped cuprate superconductors.^[38] The dispersive direction of the quasi 1D surface bands correspond to the direction of the charge/orbital stripes, and the Fermi arcs created by the surface bands are perpendicular to the charge/orbital stripes as schematically shown in **Figure 1b**.^[34–36] As the band structure is sensitive to the charge/orbital order, angle-resolved photoemission spectromicroscopy is a unique technique to study if such an order occurs in domains, and if so, what is the domain dependent electronic structure of IrTe_2 . Here, it is worth noting that very recently, the technique has been successfully applied to study facet dependent surface states in weak^[39] or higher order^[40] topological insulators. In addition, it is highly interesting to observe spin polarization of the surface states by means of spin-resolved angle-resolved photoemission spectroscopy (SARPES). However, the spin-resolved measurements require large photon flux which is technically difficult in the focused beam for the photoemission spectromicroscopy experiments. Therefore, it is currently impossible to resolve spins in the angle-resolved photoemission spectromicroscopy. Instead, once the relationship between the charge/orbital order and the surface states is established by angle-resolved photoemission spectromicroscopy, one may try to create a domain large enough for SARPES. In the present work, we follow this strategy and study IrTe_2 by means of angle-resolved photoemission spectromicroscopy and SARPES.

2. Evolution From Striped Domains to Trijunction Domains

Figure 1c shows the photoemission spectromicroscopy image of the entire single crystal of IrTe_2 taken at 250 K. The crystal was cleaved at 300 K and slowly cooled across the phase transition temperature of 280 K. The zoomed view is shown in **Figure 1d**. The image shows striped domains of length ≈ 50 – 100 μm . The intensity of each pixel reflects the spectral change due to the first order phase transition, and the high intensity (bright) and low intensity (dark) regions may correspond to the different directions of the charge/orbital stripes among the three possible directions. **Figure 1e–g** exhibits temperature evolution of the striped domains with cooling. Here, the cooling rate is set to ≈ 2 K min^{-1} that is slow enough to allow formation of the low temperature phase. Apparently, the domain contrast is weak at 47 K. This indicates morphological change of the domain texture between 250 and 47 K which will be discussed in the following paragraphs. After the observation, the sample was warmed to 290 K where the spectromicroscopy image hardly shows any appreciable structures (**Figure 1h**).

Figure 2a,b shows photoemission spectromicroscopy images and photoemission spectra of selected points for 290 K. At 290 K above the transition temperature, the system is homogeneous with a single photoemission spectrum. At 250 K below the transition temperature, the striped domains are observed and only two types of photoemission spectra are seen as in **Figure 2c,d** although three different directions of the anisotropic charge/orbital order are expected in the triangular lattice. On the other hand, at 47 K, three types of photoemission spectra are observed, consistent with the three directions of the charge/orbital order (**Figure 2e,f**). The lower temperature bulk

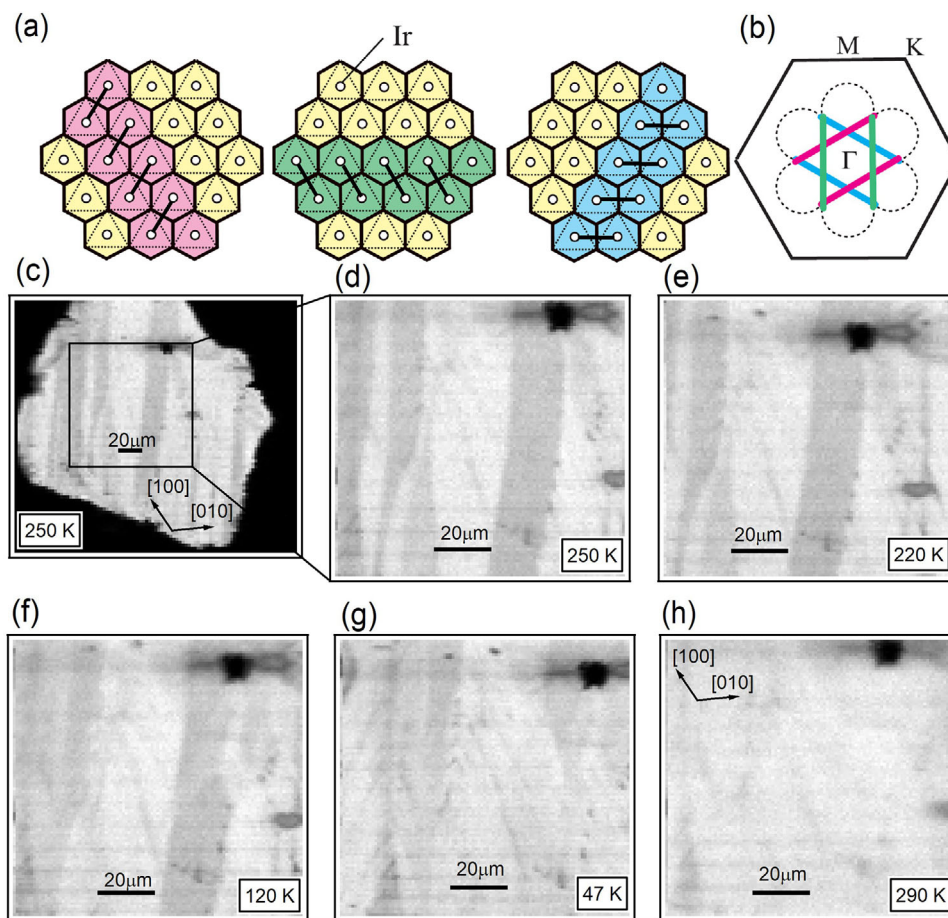


Figure 1. Charge/orbital stripes in IrTe_2 and appearance of striped domains. a) Three directions of the charge/orbital stripes in the IrTe_2 layer. An Ir–Ir dimer is represented by two Ir sites connected by a thick line. The Ir–Ir dimers form the stripes running along one of the trigonal axes. b) Three directions of the Fermi arcs in the Brillouin zone corresponding to the three directions of the charge/orbital stripes. The dotted curves schematically show the bulk Fermi surfaces. c) Photoemission intensity image of the wide area at 250 K. The images were obtained by integrating the photoemission spectra from the Fermi level to -2.3 eV below it since the spectrum of IrTe_2 in this energy range is known to change dramatically across the phase transition. d) Photoemission intensity image of the selected area indicated by the box in (c) at 250 K. e–g) Photoemission intensity images of the selected area at 220, 120, and 47 K taken in the cooling process. The cooling rate is $\approx 2 \text{ K min}^{-1}$. h) Photoemission intensity image of the selected area at 290 K after the heating from 47 K. All the images were taken at $h\nu = 27 \text{ eV}$ with linear polarization (horizontal). The crystals axes shown in (h) are common for (d–g).

phase transition at 180 K is accompanied by periodicity change of the charge/orbital order from $(5 \times 1 \times 5)$ to $(8 \times 1 \times 8)$ with cooling.^[27–29,32] In addition, it has been reported that the surface structure changes from the high temperature (5×1) phase to the low temperature (8×1) phase with contribution of the (6×1) phase in the intermediate temperature range.^[31] The periodicity change would drive the domains structure to evolve dramatically.

The domain structure is expected to depend on the cooling rate as shown in Figure S2a,b, Supporting Information. Figure S2a,b, Supporting Information displays a photoemission spectroscopy image for the sample quenched quickly to 47 K after cleavage at 300 K and that for the sample cleaved at 47 K after quenching from 300 K. The major domains have irregular shapes and are much larger in size than those seen for the slow cooling. In the quenched cases, one of the three directions is selected and frozen at the phase transition. While the Fermi surfaces of the major domains are clearly observed (Figure S2c,e, Supporting Information), those of the minor domains are very broad (Fig-

ure S2d,f, Supporting Information). These observations indicate that the charge/orbital stripes are highly disordered in the minor domains, similar to the situation of quenched glasses. The present observation suggests that the anisotropic surface state can be controlled and manipulated by domain engineering in IrTe_2 .

Among the three types of photoemission spectra in Figure 2f, the intensity around -0.9 eV is higher in one of the three types while the intensity around -1.5 eV is enhanced in another type of photoemission spectra. Therefore, the two out of the three kinds of domains can be identified by using energy windows α and β (indicated by the double-headed arrows in Figure 2f) which include -0.9 and -1.5 eV , respectively. Figure 3a,b shows images at 47 K which are obtained by the energy windows. These images allow us to draw boundaries of the three kinds of domains as shown by solid lines in Figure 3c. The domains labeled as #3 are highlighted with window α (Figure 3a) while those labeled as #1 are highlighted with window β (Figure 3b). Figure 3d,e,f

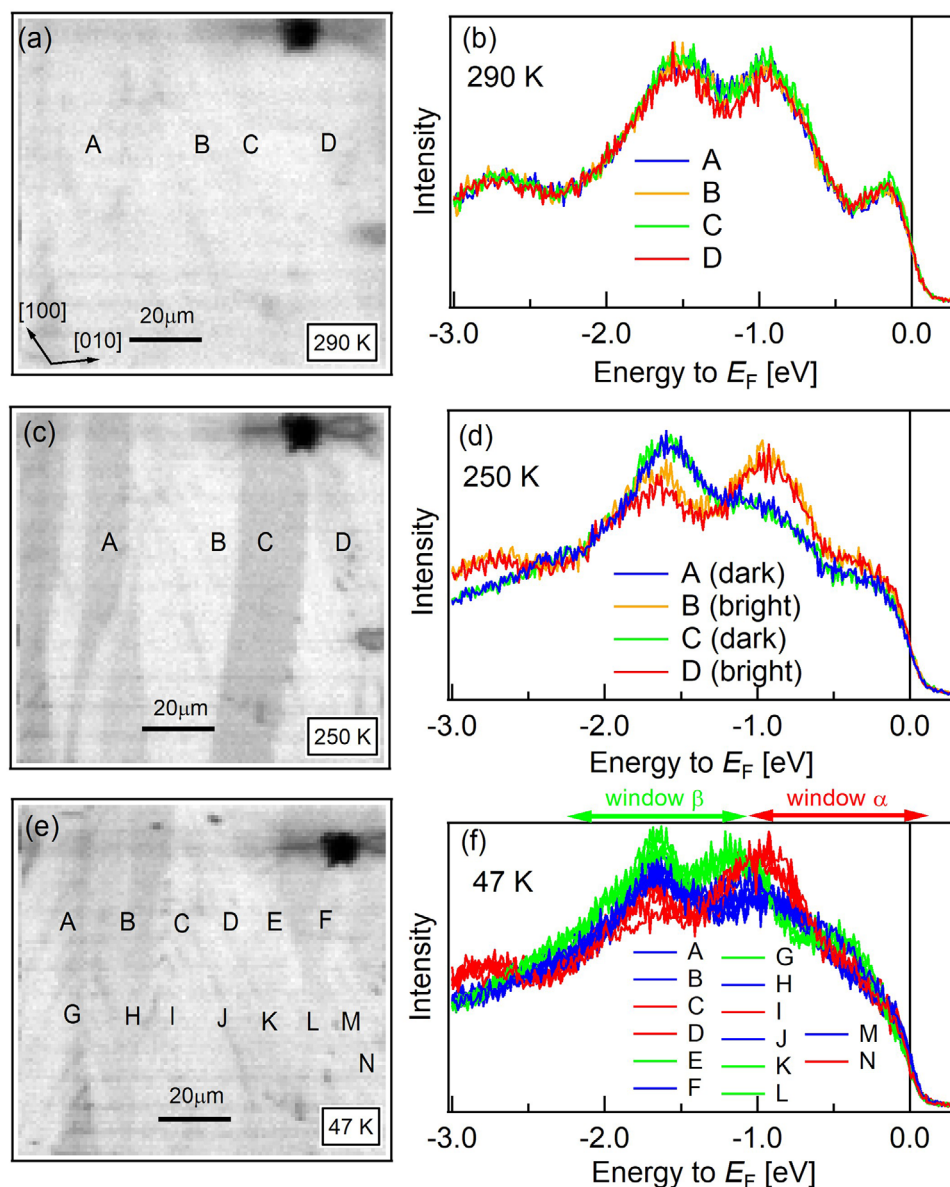


Figure 2. Domain dependent photoemission spectra. a) Domain structure and b) photoemission spectra at 290 K which is above the transition temperature. c) Domain structure and d) photoemission spectra at 250 K which is below the transition temperature. e) Domain structure and f) photoemission spectra at 47 K. The images and spectra were taken at $h\nu = 27$ eV with linear polarization (horizontal).

shows Fermi surfaces measured at the three points (indicated by the crosses in Figure 3c) belonging to the different domains. The electronic anisotropy can be recognized by their shapes. In addition to the Fermi surfaces from the bulk, Fermi arcs derived from the surface bands are observed for each domain. The surface bands in domain #1 are dispersive along the direction of the horizontal charge/orbital stripes and exhibit the Fermi arcs perpendicular to them as indicated by the broken lines in Figure 3d. Compared with the sharp Fermi arcs for domain #1, the Fermi arcs of domains #2 and #3 are blurred although their anisotropic shape can be recognized as indicated by the broken lines in Figure 3e,f. Most likely, the charge/orbital stripes are well established in newly developed domain #1 whereas they are somewhat disordered in domains #2 and #3 during the evolution from

“the intermediate temperature fivefold stripe phase” to “the low temperature sixfold or eightfold stripe phase”.^[27–30,32] The striped domain pattern in the intermediate temperature range is characterized by the two directions of electronic stripes which form $\approx 60^\circ$ and are truncated at the boundary as shown in Figure 3g. Although it is observed at 250 K in the present experiment, this situation corresponds to the domain boundary observed by Maurer et al. at 180 K.^[30]

3. Spin Polarization of the Surface States

The Fermi arcs are mainly constructed from the Ir 5d and Te 5p orbitals at the surface layer. Therefore, the Fermi arcs may exhibit spin polarization induced by the broken inversion symmetry

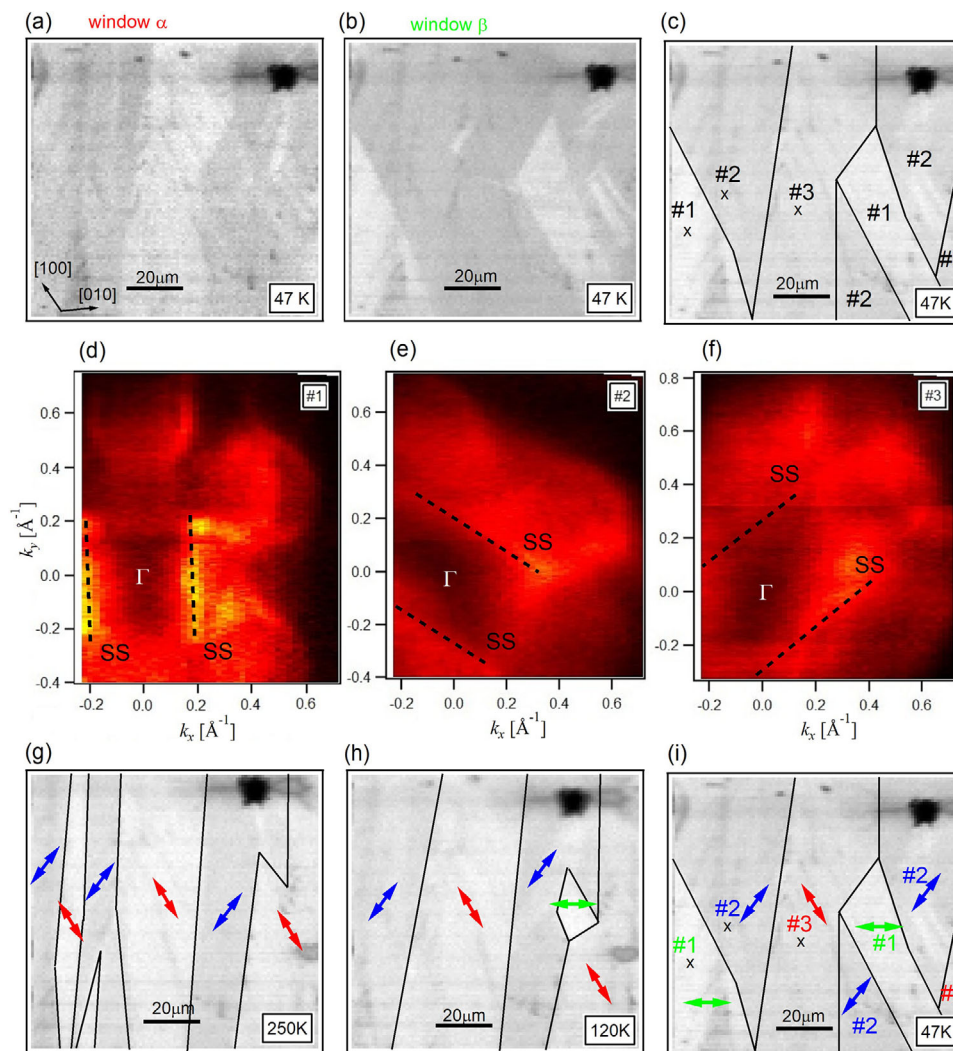


Figure 3. Domain dependent Fermi surfaces and evolution from striped to trijunction domains. a) Domain texture at 47 K visualized by energy window α of Figure 2f. b) Domain texture at 47 K visualized by energy window β of Figure 2f. c) Domain boundaries at 47 K determined from the images with different energy windows. d–f) Fermi surfaces of the three different domains at 47 K. The broken lines indicate Fermi arcs derived from the surface states (SS). g–i) Domain textures at 250, 120, and 47 K. All the images were taken at $h\nu = 27$ eV with linear polarization (horizontal). The solid lines indicate domain boundaries. The arrows indicate the directions of charge/orbital stripes.

and the strong spin–orbit interaction of Ir 5d and Te 5p. Indeed, the Fermi arcs of the striped phase have a peculiar spin texture as explained below. **Figure 4a** shows a Fermi surface map taken at 300 K in which momentum points for SARPES are plotted. Band dispersions along the horizontal axis (k_x axis) for 300 and 20 K are plotted in Figure 4b. At 20 K, the surface bands dispersive along the k_x axis are observed as indicated by the broken lines. The surface bands create Fermi arcs which are perpendicular to the k_x axis. This observation indicates that the sample surface is dominated by domains with horizontal stripes. As the crystal was cleaved at 300 K and then rapidly cooled to 20 K with a cooling rate of 20–30 K min^{−1}, the situation is close to the quenched case shown in Figure S2a, Supporting Information. When the sample surface is dominated by the domain with horizontal stripes as shown in Figure S2a, Supporting Information, the Fermi arcs along the vertical direction are clearly observed as

shown in Figure S2c, Supporting Information. Figure 4c shows out-of-plane spin polarization maps which are created from the SARPES spectra taken at 20 K with linearly polarized light as shown in Figure S3, Supporting Information. In the left panel of Figure 4c, the out-of-plane spin polarization is plotted as a function of k_x (across the Fermi arc) and energy. The momentum positions for the spin-polarization maps are indicated by the open triangles in Figure 4a. The surface band creating the Fermi arc clearly shows negative spin polarization for the positive k_x as indicated by the broken line in Figure 4c. In addition to the surface band creating the Fermi arcs at E_F , the spectral features around −0.5 eV and −1.2 eV show appreciable spin polarization. The spin polarization around −0.5 eV is negative (positive) for the positive (negative) k_x while that around −1.2 eV is positive (negative) for the positive (negative) k_x . Although possibility of surface band origin cannot be excluded, these features would be

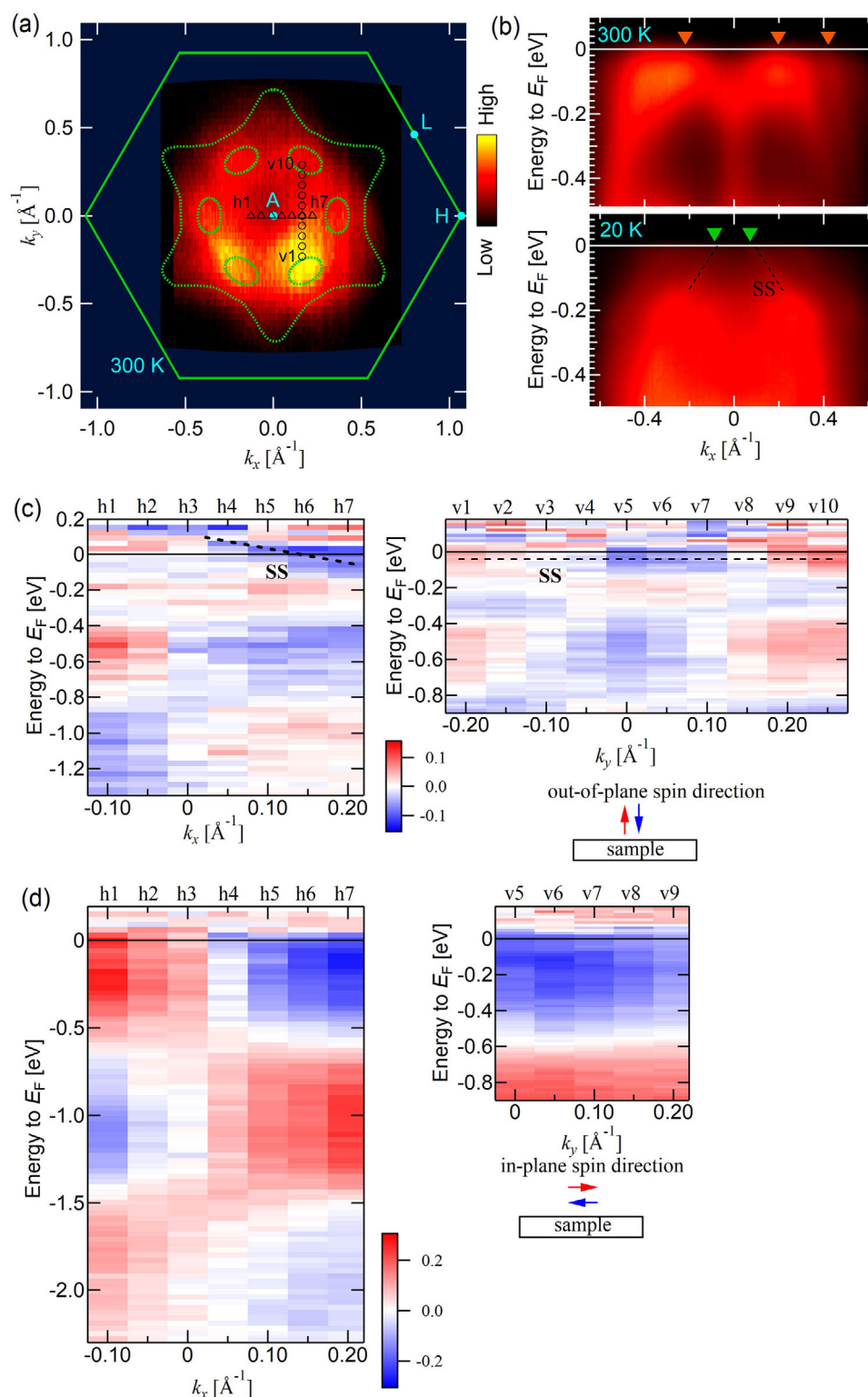


Figure 4. Spin texture of the surface and bulk bands. a) Fermi surface map taken at 300 K with $h\nu = 23$ eV. The dotted curves indicate the theoretically predicted Fermi surfaces.^[20] Momentum points for SARPES measurements are indicated by the open triangles and circles. b) Band maps along the horizontal cut at 300 and 20 K. At 20 K, the surface bands cross E_F as indicated by the broken lines and the green triangles. c) Out-of-plane spin-polarization maps across and along the Fermi arc. The broken line indicates the surface band. Positive and negative spin polarizations are indicated by red and blue colors. d) In-plane spin-polarization maps across and along the Fermi arc.

derived from the Rashba type splitting of the bulk bands. Possibility of bulk inversion symmetry breaking will be discussed in the last paragraph of this section. In the right panel of Figure 4c, the out-of-plane spin polarization is plotted as a function of k_y (along the Fermi arc) and energy. The momentum positions for the spin-polarization maps are indicated by the open circles in Figure 4a. Interestingly, the out-of-plane spin polarization of the surface band indicated by the broken line changes its sign along the Fermi arc. Around $k_y \approx \pm 0.2 \text{ \AA}^{-1}$, the spin direction is outward from the surface while the spin is inwardly oriented around $k_y \approx 0.0 \text{ \AA}^{-1}$.

The charge/orbital stripes of each IrTe_2 plane are stacked in a staircase-type pattern along the c -axis, creating the tilted unit cell and the corresponding Brillouin zone (Figure S1a, Supporting Information). According to the calculations by Pascut et al. and Toriyama et al., the stacked charge/orbital stripes form new conducting layers which are tilted from the IrTe_2 plane.^[25–27] Near E_F , the Ir 5d and Te 5p bands are dispersive along this conducting layer forming quasi 2D Fermi surfaces. As the conducting layer is truncated at the cleaved surface, the Fermi arcs can be viewed as edge states of the conducting layer. The observation of out-of-plane spin polarization suggests that the spin direction at the edge of the conducting layer can be tilted with respect to the original IrTe_2 plane. It is highly challenging to reproduce the spin polarized surface band by theoretical calculations. It has not been reproduced even in the most recent and sophisticated calculation using a slab geometry by Rumo et al.^[36] In addition, it has not been observed in the recent nano-ARPES study by Bao et al.^[41]

Figure 4d shows in-plane spin-polarization maps which are created from the SARPES spectra taken at 20 K with linearly polarized light in Figure S4, Supporting Information. Strong spin polarization is observed in the energy windows from E_F to -0.4 eV and from -0.8 eV to -1.3 eV . The surface band creating the Fermi arc is buried in the spin polarized band from E_F to -0.4 eV . The spin polarization in this energy range changes its sign between the positive and negative k_x regions, suggesting Rashba-type spin splitting. The theoretical study by Pascut et al. predicts inversion symmetry breaking of the $(3n+2)$ -fold charge/orbital stripe phase with even n .^[27] If the 8-fold stripe phase with $n = 2$ is realized, the observed in-plane spin polarizations can be assigned to spin-momentum locking of the bulk bands. The theoretically predicted Rashba splitting is $\approx 0.1 \text{ eV}$ along the $\Gamma'Z'$ direction and may not be compatible with the observation which suggests the splitting as large as 0.5 eV . (The Z' point is indicated in the lower right panel of Figure S1a, Supporting Information.) However, the $\Gamma'Z'$ cut is not covered in the present measurements, and the Rashba splitting would be enhanced in the measured momentum regions. In addition, it is possible that stripe phases with various n are mixed into the 6-fold stripe phase with inversion symmetry and that the even n states among them contribute to the spin polarization. Considering these uncertainties, we cannot exclude the possibility that the observed spin polarization is derived from the bulk Rashba splitting. On the other hand, the in-plane polarization would be assigned to surface bands. In the energy range from E_F to -0.4 eV , the energy gap is formed between the $p_x \pm ip_y$ type orbital state due to the Te 5p spin-orbit coupling.^[42] Therefore, the in-plane spin polarization can be explained if the surface state is

formed within the energy gap. As for the energy range from -0.8 to -1.3 eV , the observed spin polarized band would be associated with the surface band predicted in the calculation by Rumo et al.^[36]

4. Conclusion

In summary, using angle-resolved photoemission spectroscopy, we have shown that the stripe-type charge/orbital order in IrTe_2 is accompanied by mesoscopic striped domains. The striped domain texture at 250 K is obtained by the two directions of the charge/orbital stripes forming $\approx 60^\circ$ at the boundary. The striped domain of the electronic stripe phase can be stabilized under the anisotropic strain from the neighboring domains. At 47 K, the striped texture is replaced by the trijunction texture of the three types of domains with different charge/orbital stripe directions. On the other hand, the formation of the striped or trijunction texture is suppressed in the quenched case. Each domain harbors the anisotropic surface states forming the Fermi arcs with peculiar spin polarization. The Fermi arcs correspond to the edge states of the 2D bulk electronic bands which are truncated at the cleaved surface. IrTe_2 is very unique in that the spin polarized surface states are correlated with the charge/orbital stripe domain textures. We anticipate that the domain boundary in IrTe_2 is a new playground to explore a novel low-dimensional electronic state under the strong spin-orbit interaction with a possible impact on nanoscale electronic/magnetic devices.

5. Experimental Section

Synthesis and Characterization: Single crystal samples of IrTe_2 were prepared using a self-flux as reported in the literature.^[14] The single crystal samples were characterized by transport,^[14] X-ray diffraction,^[25] and angle-resolved photoemission^[22] measurements.

Angle-Resolved Photoemission Spectromicroscopy: The angle-resolved photoemission spectroscopy results were obtained at the spectromicroscopy beamline, Elettra synchrotron facility, Italy.^[43] Photons at 27 eV were focused through a Schwarzschild objective in order to obtain a sub-micron size beam spot. For the present measurements, the total energy resolution was set to $\approx 50 \text{ meV}$ and the angle resolution was 1° . The measurements were performed under ultra-high vacuum in the 10^{-10} Torr range on in situ prepared surfaces. The microscopy images were obtained by integrating the photoemission spectra in appropriate energy windows. The photoemission spectra are angles integrated with the acceptance angle of $\pm 7.5^\circ$ corresponding to $\pm 0.3 \text{ \AA}^{-1}$ around the Γ point along the ΓM direction.

Spin-Resolved Angle-Resolved Photoemission Spectroscopy: Spin-resolved angle-resolved photoemission spectroscopy (SARPES) measurements were performed at beamline 9B of Hiroshima Synchrotron Radiation Center (HiSOR). The beam spot size is $\approx 2.0 \text{ mm} \times 0.9 \text{ mm}$. The base pressure of the spectrometer was in the 10^{-11} Torr range. The crystals were cleaved at 300 K under the ultrahigh vacuum and then cooled to 20 K for the SARPES measurements. The SARPES data were obtained within 12 h after the cleavage. The total energy resolution was set to 51 meV for excitation energy $h\nu$ of 23 eV. Binding energies were calibrated using the Fermi edge of gold reference samples.

Supporting Information

Supporting Information is available from the Wiley Online Library or from the author.

Acknowledgements

The authors would like to thank D. I. Khomskii, A. Damascelli, A. Fujimori, and H.-J. Noh for valuable discussions and D. Ootsuki and M. Horio for contributions to the experiments in the early stage of this work. The authors also thank J. Jia for assisting during a part of the experiments. This work was partially supported by Grants-in-Aid from the Japan Society of the Promotion of Science (JSPS) (Grants No. 26287082, 25400356, JP16H02114, JP19H05823, JP22H01182, and JP19H00659), and CREST, Japan Science and Technology Agency (Grant No. JPMJCR15Q2). The SARPES experiments (Proposal No. 15-A-6) were performed with the approval of the Proposal Assessing Committee of the Hiroshima Synchrotron Radiation Center. This work was supported by the joint research program of ZAIKEN, Waseda University (Project No. 31010).

Conflict of Interest

The authors declare no conflict of interest.

Author Contributions

Designed and coordinated the study: N.S. and T.M. Synthesized the single crystals of IrTe_2 : S.P., H.I., K.K., and M.N. Performed angle-resolved photoemission spectromicroscopy experiments at SPECTROMICROSCOPY-3.2L beamline of Elettra which is managed by A.B.: N.S., T.M., R.M., V.K., A.G., and A.B. Analyzed the data: A.B., Y.O., and T.M. Performed spin-resolved angle-resolved photoemission experiments at BL-9B of HiSOR which is managed by K.M. and T.O.: T.M., Y.O., K.T., K.M., and T.O. Wrote the paper: N.S., A.B., T.O., and T.M.. All authors discussed the results and commented on the manuscript.

Data Availability Statement

The data that support the findings of this study are available from the corresponding author upon reasonable request.

Keywords

charge order, orbital order, spin-momentum locking, striped domains, transition-metal dichalcogenides

Received: March 15, 2022
Revised: June 13, 2022
Published online: July 10, 2022

- [1] T. Choi, Y. Horibe, H. T. Yi, Y. J. Choi, W. Wu, S.-W. Cheong, *Nat. Mater.* **2010**, *9*, 253.
- [2] M. Kronseider, M. Buchner, H. G. Bauer, C. H. Back, *Nat. Commun.* **2013**, *4*, 2054.
- [3] F. P. Chmiel, N. W. Price, R. D. Johnson, A. D. Lamirand, J. Schladt, G. van der Laan, D. T. Harris, J. Irwin, M. S. Rzechowski, C.-B. Eom, P. G. Radaelli, *Nat. Mater.* **2018**, *17*, 581.
- [4] E. Y. Ma, Y.-T. Cui, K. Ueda, S. Tang, K. Chen, N. Tamura, P. M. Wu, J. Fujioka, Y. Tokura, Z.-X. Shen, *Science* **2015**, *350*, 538.
- [5] Y. Zhang, H. Lu, X. Yan, X. Cheng, L. Xie, T. Aoki, L. Li, C. Heikes, S. P. Lau, D. G. Schlom, L. Chen, A. Gruverman, J. Pan, *Adv. Mater.* **2019**, *31*, 1902099.
- [6] Y.-L. Huang, L. u Zheng, P. Chen, X. Cheng, S.-L. Hsu, T. Yang, X. Wu, L. Ponet, R. Ramesh, L.-Q. Chen, S. Artyukhin, Y.-H. Chu, K. Lai, *Adv. Mater.* **2020**, *32*, 1905132.
- [7] S. Lupi, L. Baldassarre, B. Mansart, A. Perucchi, A. Barinov, P. Dudin, E. Papalazarou, F. Rodolakis, J. -P. Rueff, J. -P. Itié, S. Ravy, D. Nicoletti, P. Postorino, P. Hansmann, N. Parragh, A. Toschi, T. Saha-Dasgupta, O. K. Andersen, G. Sangiovanni, K. Held, M. Marsi, *Nat. Commun.* **2010**, *1*, 105.
- [8] D. D. Sarma, D. Topwal, U. Manju, S. R. Krishnakumar, M. Bertolo, S. La Rosa, G. Cautero, T. Y. Koo, P. A. Sharma, A. Fujimori, *Phys. Rev. Lett.* **2004**, *93*, 097202.
- [9] C. A. Jenkins, A. Scholl, R. Kainuma, H. J. Elmers, T. Otori, *Appl. Phys. Lett.* **2012**, *100*, 032401.
- [10] P. G. Radaelli, Y. Horibe, M. J. Gutmann, H. Ishibashi, C. H. Chen, R. M. Ibberson, Y. Koyama, Y. S. Hor, V. Kirykhin, S. W. Cheong, *Nature* **2002**, *416*, 155.
- [11] D. I. Khomskii, T. Mizokawa, *Phys. Rev. Lett.* **2005**, *94*, 156402.
- [12] S. Jobic, P. Deniard, R. Brec, J. Rouxel, A. Jouanneaux, A. N. Fitch, *Z. Anorg. Allg. Chem.* **1991**, *598*, 199.
- [13] N. Matsumoto, K. Taniguchi, R. Endoh, H. Takano, S. Nagata, *J. Low Temp. Phys.* **1999**, *117*, 1129.
- [14] S. Pyon, K. Kudo, M. Nohara, *Phys. C* **2013**, *494*, 80.
- [15] S. Pyon, K. Kudo, M. Nohara, *J. Phys. Soc. Jpn.* **2012**, *81*, 053701.
- [16] J. J. Yang, Y. J. Choi, Y. S. Oh, A. Hogan, Y. Horibe, K. Kim, B. I. Min, S.-W. Cheong, *Phys. Rev. Lett.* **2012**, *108*, 116402.
- [17] D. Ootsuki, Y. Wakisaka, S. Pyon, K. Kudo, M. Nohara, M. Arita, H. Anzai, H. Namatame, M. Taniguchi, N. L. Saini, T. Mizokawa, *Phys. Rev. B* **2012**, *86*, 014519.
- [18] A. F. Fang, G. Xu, T. Dong, P. Zheng, N. L. Wang, *Sci. Rep.* **2013**, *3*, 1153.
- [19] Y. S. Oh, J. J. Yang, Y. Horibe, S.-W. Cheong, *Phys. Rev. Lett.* **2013**, *110*, 127209.
- [20] H. Cao, B. C. Chakoumakos, X. Chen, J. Yan, M. A. McGuire, H. Yang, R. Custelcean, H. D. Zhou, D. J. Singh, D. Mandrus, *Phys. Rev. B* **2013**, *88*, 115122.
- [21] B. Joseph, M. Bende, L. Simonelli, L. Mauger, S. Pyon, K. Kudo, M. Nohara, T. Mizokawa, N. L. Saini, *Phys. Rev. B* **2013**, *88*, 224109.
- [22] D. Ootsuki, S. Pyon, K. Kudo, M. Nohara, M. Arita, H. Anzai, H. Namatame, M. Taniguchi, N. L. Saini, T. Mizokawa, *J. Phys. Soc. Jpn.* **2013**, *82*, 093704.
- [23] K. Kim, S. Kim, K.-T. Ko, H. Lee, J.-H. Park, J. J. Yang, S.-W. Cheong, B. I. Min, *Phys. Rev. Lett.* **2015**, *114*, 136401.
- [24] A. Kiswandhi, J. S. Brooks, H. B. Cao, J. Q. Yan, D. Mandrus, Z. Jiang, H. D. Zhou, *Phys. Rev. B* **2013**, *87*, 121107(R).
- [25] T. Toriyama, M. Kobori, Y. Ohta, T. Konishi, S. Pyon, K. Kudo, M. Nohara, K. Sugimoto, T. Kim, A. Fujiwara, *J. Phys. Soc. Jpn.* **2014**, *83*, 033701.
- [26] G. L. Pascut, K. Haule, M. J. Gutmann, S. A. Barnett, A. Bombardi, S. Artyukhin, T. Birol, D. Vanderbilt, J. J. Yang, S.-W. Cheong, V. Kiryukhin, *Phys. Rev. Lett.* **2014**, *112*, 086402.
- [27] G. L. Pascut, T. Birol, M. J. Gutmann, J. J. Yang, S.-W. Cheong, K. Haule, V. Kiryukhin, *Phys. Rev. B* **2014**, *90*, 195122.
- [28] P.-J. Hsu, T. Mauerer, M. Vogt, J. J. Yang, Y. S. Oh, S.-W. Cheong, M. Bode, W. Wu, *Phys. Rev. Lett.* **2013**, *111*, 266401.
- [29] K.-T. Ko, H.-H. Lee, D.-H. Kim, J. J. Yang, S.-W. Cheong, M. J. Eom, J. S. Kim, R. Gammag, K.-S. Kim, H.-S. Kim, T.-H. Kim, H. W. Yeom, T.-Y. Koo, H.-D. Kim, J.-H. Park, *Nat. Commun.* **2015**, *6*, 7342.
- [30] T. Mauerer, M. Vogt, P.-J. Hsu, G. L. Pascut, K. Haule, V. Kiryukhin, J. Yang, S.-W. Cheong, W. Wu, M. Bode, *Phys. Rev. B* **2016**, *94*, 014106.
- [31] H. S. Kim, S. Kim, K. Kim, B. I. Min, Y.-H. Cho, L. Wang, S.-W. Cheong, H. W. Yeom, *Nano Lett.* **2016**, *16*, 4260.
- [32] K. Takubo, K. Yamamoto, Y. Hirata, H. Wadati, T. Mizokawa, R. Sutarto, F. He, K. Ishii, Y. Yamasaki, H. Nakao, Y. Murakami, G. Matsuo, H. Ishii, M. Kobayashi, K. Kudo, M. Nohara, *Phys. Rev. B* **2018**, *97*, 205142.
- [33] H. Oike, K. Takeda, M. Kamitani, Y. Tokura, F. Kagawa, *Phys. Rev. Lett.* **2021**, *127*, 145701.

- [34] D. Ootsuki, H. Ishii, K. K. Kudo, M. Nohara, M. Arita, H. Namatame, M. Taniguchi, N. L. Saini, T. Mizokawa, *J. Phys. Chem. Solids* **2019**, 128, 270.
- [35] D. Ootsuki, H. Ishii, K. Kudo, M. Nohara, M. Takahashi, M. Horio, A. Fujimori, T. Yoshida, M. Arita, H. Anzai, H. Namatame, M. Taniguchi, N. L. Saini, T. Mizokawa, *J. Phys. Soc. Jpn.* **2017**, 86, 123704.
- [36] M. Rumo, C. W. Nicholson, A. Pulkkinen, B. Hildebrand, G. Kremer, B. Salzmänn, M.-L. Mottas, K. Y. Ma, E. L. Wong, M. K. L. Man, K. M. Dani, B. Barbiellini, M. Muntwiler, T. Jaouen, F. O. von Rohr, C. Monney, *Phys. Rev. B* **2020**, 101, 235120.
- [37] C. W. Nicholson, M. Rumo, A. Pulkkinen, G. Kremer, B. Salzmänn, M. Mottas, B. Hildebrand, T. Jaouen, T. K. Kim, S. Mukherjee, K. Ma, M. Muntwiler, F. O. von Rohr, C. Cacho, C. Monney, *Commun. Mater.* **2021**, 2, 25.
- [38] T. Yoshida, X. J. Zhou, T. Sasagawa, W. L. Yang, P. V. Bogdanov, A. Lanzara, Z. Hussain, T. Mizokawa, A. Fujimori, H. Eisaki, Z.-X. Shen, T. Kakeshita, S. Uchida, *Phys. Rev. Lett.* **2003**, 91, 027001.
- [39] R. Noguchi, T. Takahashi, K. Kuroda, M. Ochi, T. Shirasawa, M. Sakano, C. Bareille, M. Nakayama, M. D. Watson, K. Yaji, A. Hara-sawa, H. Iwasawa, P. Dudin, T. K. Kim, M. Hoesch, V. Kandyba, A. Giampietri, A. Barinov, S. Shin, R. Arita, T. Sasagawa, T. Kondo, *Nature* **2019**, 566, 518.
- [40] R. Noguchi, M. Kobayashi, Z. Jiang, K. Kuroda, T. Takahashi, Z. Xu, D. Lee, M. Hirayama, M. Ochi, T. Shirasawa, P. Zhang, C. Lin, C. Bareille, S. Sakuragi, H. Takaka, S. Kunisada, K. Kurokawa, K. Yaji, A. Hara-sawa, V. Kandyba, A. Giampietri, A. Barinov, T. K. Kim, C. Cacho, M. Hashimoto, D. Lu, S. Shin, R. Arita, K. R. Lai, T. Sasagawa, et al., *Nat. Mater.* **2021**, 20, 473.
- [41] C. Bao, H. Zhang, Q. Li, S. Zhou, H. Zhang, K. Deng, K. Zhang, L. Luo, W. Yao, C. Chen, J. Avila, M. C. Asensio, Y. Wu, S. Zho, *Commun. Phys.* **2021**, 4, 229.
- [42] D. Ootsuki, T. Toriyama, M. Kobayashi, S. Pyon, K. Kudo, M. Nohara, T. Sugimoto, T. Yoshida, M. Horio, A. Fujimori, M. Arita, H. Anzai, H. Namatame, M. Taniguchi, N. L. Saini, T. Konishi, Y. Ohta, T. Mizokawa, *J. Phys. Soc. Jpn.* **2014**, 83, 033704.
- [43] P. Dudin, P. Lacovig, C. Fava, E. Nicolini, A. Bianco, G. Cautero, A. Barinov, *J. Synchrotron Radiat.* **2010**, 17, 445.